

# Localized structures as spatial hosts for unstable modes

A. LAMPERT<sup>1</sup> and E. MERON<sup>1,2</sup>

<sup>1</sup> *Department of Physics, Ben-Gurion University - Beer-Sheva 84105, Israel*

<sup>2</sup> *Department of Solar Energy and Environmental Physics, BIDR, Ben-Gurion University - Sede Boqer Campus 84990, Israel*

received 5 December 2006; accepted in final form 20 February 2007

published online 23 March 2007

PACS 47.54.-r – Pattern selection; pattern formation

PACS 05.45.-a – Nonlinear dynamics and chaos

PACS 82.40.Bj – Oscillations, chaos, and bifurcations

**Abstract** – We study spatially extended systems undergoing Hopf-Turing instabilities to temporal oscillations and periodic spatial patterns, focusing on mono-stability regimes where one mode nonlinearly damps the other. Using the pertinent normal-form equations, we identify a new type of instability beyond which localized structures of the dominant mode host the unstable, nonlinearly damped mode. Thus, stationary localized structures of the Turing mode can lose stability to breathing structures that host the Hopf mode, and propagating localized structures of the Hopf mode can lose stability to stationary structures hosting the Turing mode. Hosting instabilities of this kind are expected to be found in other multi-mode systems as well. Potential applications include self-organized waveguides, and data storage.

Copyright © EPLA, 2007

The dynamics of spatially extended systems far from thermal equilibrium often involve competing modes [1]. The modes may appear in multiple instabilities or represent different populations in biological communities [2]. Multiple instabilities have been observed in various systems including thermal fluid convection [3], parametrically excited surface waves [4], chemical reactions [5] and optical systems [6]. Dynamical behaviors that have been identified in such systems include mono-stability of a single pure-mode state, multi-stability of pure-mode states, mixed mode states, oscillatory competition, chaotic dynamics and others [3–7].

The behavior of a multi-mode system in a mono-stability regime, where a single mode damps all other modes, resembles in many respects the behavior of the corresponding single-mode system. For example, the behavior of a system that goes through both Hopf and Turing<sup>1</sup> bifurcations, but is tuned to the mono-stability range of the Turing mode, shows stationary spatial patterns (*e.g.* stripes and hexagons) indistinguishable from the patterns exhibited by a single-mode system that merely goes through a Turing bifurcation. It is, perhaps, for this reason that most studies of multi-mode systems focused on other dynamical regimes, primarily the regimes of multi-stability and of mixed modes, where

<sup>1</sup>We use the term “Turing bifurcation” to describe a finite-wavenumber stationary instability in general [1].

spatiotemporal structures and dynamical behaviors involving different modes have been found.

In this letter we focus on mono-stability ranges of multi-mode systems and show that localized structures of stable pure modes can host unstable modes. Specifically, we find instabilities of pure-mode localized structures, such as defects in stationary Turing patterns, that give rise to multi-mode structures, such as breathing defects, involving locally both the Turing and the Hopf modes. To study this type of instability we consider systems whose homogeneous stationary states lose stability both to stationary periodic patterns and to uniform temporal oscillations in a Hopf-Turing bifurcation (hereafter “Hopf-Turing” systems). We further assume, in most of the cases considered here, that the systems are subjected to spatial and/or temporal periodic forcing. These types of forcing significantly increase the variety of localized structures Hopf-Turing systems can support and help demonstrating the hosting phenomenon.

Spatial forcing with a wavenumber,  $k_f$ , about twice as large as the unforced pattern’s wavenumber,  $k_0$ , breaks the translational symmetry of the system and fix the spatial phase of the pattern at two stable values differing by  $\pi$  with respect to one another [8]. Along with these fixed-phase patterns, or “phase states”, stationary front structures appear. The fronts are bi-asymptotic to the two phase states, and thus shift the spatial phase of the

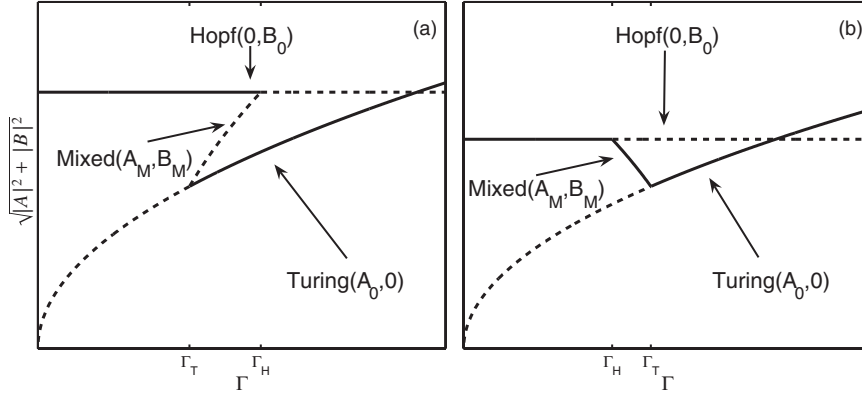


Fig. 1: Bifurcation diagrams showing stationary homogeneous solutions of eqs. (2) for (a)  $\Delta < 0$  (mixed mode is unstable) and (b)  $\Delta > 0$  (mixed mode is stable). Solid (dashed) lines denote stable (unstable) solutions. The labels  $\Gamma_T$  and  $\Gamma_H$  denote the stability thresholds of pure-Turing and pure-Hopf solutions, respectively.

pattern by  $\pi$ . These fronts go through a non-equilibrium Ising-Bloch (NIB) bifurcation, whereby a single stationary Ising front at high forcing strengths loses stability to a pair of stationary Bloch fronts, with broken chiral symmetry, at low forcing strengths [9]. In the Bloch regime stationary two-dimensional vortex structures exist. Temporal forcing, with a frequency,  $\omega_f$ , about twice as large as the oscillation frequency,  $\omega_0$ , of the unforced system similarly fixes the oscillation phase and leads to front structures that shift the phase by  $\pi$ . These fronts also go through a NIB bifurcation except that the two Bloch fronts are not stationary but rather propagate in opposite directions [9,10]. In this case, vortex cores, where one Bloch front switches to another, generate spiral waves [11].

Near the onset of a Hopf-Turing bifurcation in a system subjected to a spatially periodic force with wavenumber  $k_f = 2k_0$  and a time-periodic force with frequency  $\omega_f \approx 2\omega_0$ , a physical variable of the system can be approximated by

$$u(x, y, t) \approx u_0 + c_1 A e^{ikx} + c_2 B e^{i\omega t} + \text{c.c.}, \quad (1)$$

where  $k = k_f/2$  is the actual wavenumber of the Turing mode,  $\omega = \omega_f/2$  is the actual frequency of the Hopf mode<sup>2</sup>, and  $A$  and  $B$  are the modes' amplitudes, which satisfy the equations:

$$\begin{aligned} A_t &= \epsilon A + (2k_0 \partial_x - i \partial_y^2)^2 A - (\lambda |A|^2 + \kappa |B|^2) A + \gamma_k A^*, \\ B_t &= (\mu + i\nu) B + \alpha \nabla^2 B - (\delta |A|^2 + \beta |B|^2) B + \gamma_\omega B^*. \end{aligned} \quad (2)$$

In eqs. (2),  $\epsilon > 0$  and  $\mu > 0$  are the distances from the Turing and the Hopf instabilities of the unforced system,  $\nu = \omega_0 - \omega_f/2$  is the frequency detuning,  $\gamma_k$  and  $\gamma_\omega$  are the strengths of the spatial and temporal forcing,  $\lambda$  and  $\kappa$  are real-valued constants, and  $\alpha$ ,  $\beta$  and  $\delta$ , are complex-valued constants. The star denotes complex conjugation.

<sup>2</sup>The actual frequency  $\omega$  may differ from the frequency  $\omega_0$  of the unforced system due to frequency locking at half the forcing frequency.

Equations (2) have three types of stationary homogeneous solutions in addition to the zero solution  $(A, B) = (0, 0)$ : pure Turing state  $(A_0, 0)$ , pure Hopf state  $(0, B_0)$ , and mixed mode state  $(A_M, B_M)$ . We studied the existence and stability of these solutions for different values of  $\Gamma = \epsilon + \gamma_k$ , assuming  $\gamma_\omega = 0$ , and distinguished between two cases according to the sign of the quantity

$$\Delta \equiv \lambda \text{Re}(\beta) - \kappa \text{Re}(\delta). \quad (3)$$

When  $\Delta < 0$ , the mixed mode solution is unstable and a bistability range,  $\Gamma_T < \Gamma < \Gamma_H$ , exists where both the pure-Turing and the pure-Hopf solutions are stable (fig. 1a). When  $\Delta > 0$ , there is a range,  $\Gamma_H < \Gamma < \Gamma_T$ , where the mixed mode solution is stable, and no bistability range of pure mode solutions exists (fig. 1b).

We first consider mono-stability ranges of pure Turing solutions,  $(A, B) = (A_0, 0)$ , in a system subjected to spatial forcing only ( $\gamma_\omega = 0$ ). These ranges are given by  $\Gamma > \max\{\Gamma_H, \Gamma_T\}$ . In these ranges the pure Hopf state,  $(A, B) = (0, B_0)$ , is unstable and the mixed-mode state does not exist. There are two stable uniform pure-Turing solutions in these mono-stability ranges,  $(A, B) = (\pm\sqrt{\Gamma}, 0)$  as well as nonuniform stationary front solutions bi-asymptotic to the two uniform solutions. In analogy to the single-mode spatially forced Turing system [9], the front solutions of eqs. (2) can be of the Ising type, for which  $|A|$  vanishes at the front core, or of the Bloch type for which the moduli are bounded away from zero. We call these solutions Turing-Ising fronts and Turing-Bloch fronts. The Turing-Ising and the Turing-Bloch fronts further divide into longitudinal fronts, where the  $\pi$  phase shift is in the  $x$ -direction, and transverse fronts, where the phase shift is in the  $y$ -direction [12]. The longitudinal Turing-Ising fronts are stable for  $\gamma_k > \epsilon/3$  and  $\mu$  sufficiently small (see below), and are given by [9]

$$A = \sqrt{\Gamma} \tanh \left[ \sqrt{\frac{\Gamma}{2}} \left( \frac{x}{2k_0} \right) \right], \quad B = 0. \quad (4)$$

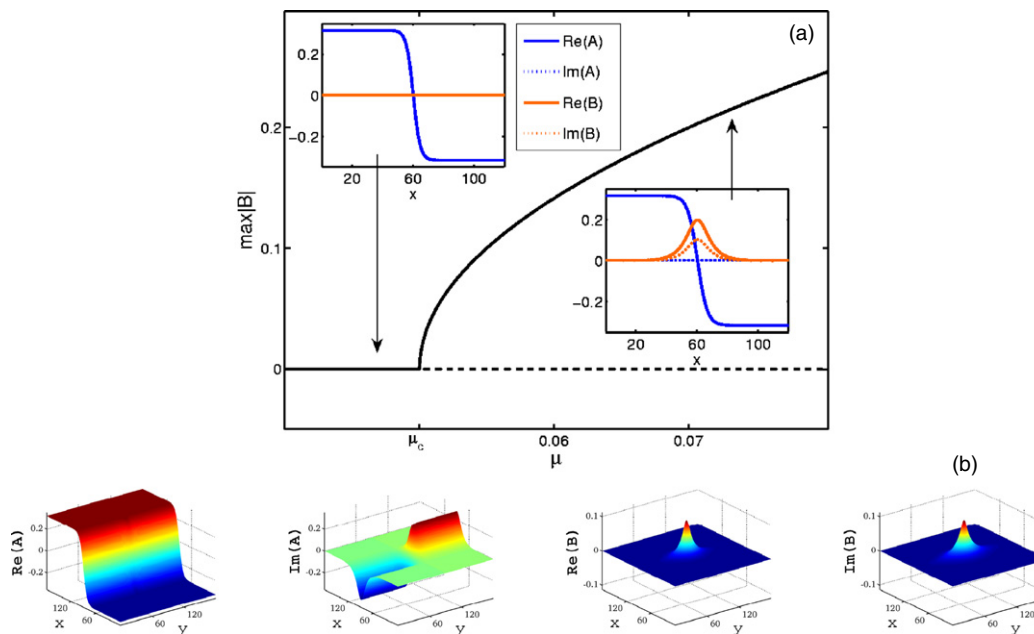


Fig. 2: Localized Turing structures as hosts of the Hopf mode. (a) A bifurcation diagram showing an instability of a stationary longitudinal Turing-Ising front to a breathing Turing-Ising front, as the distance  $\mu$  from the Hopf bifurcation of the zero state is increased. Solid (dashed) lines denote stable (unstable) solutions. The spatial front structures are shown in the two insets. Below  $\mu_c$ , the Turing mode  $A$  completely damps the Hopf mode  $B$  (left inset). Above  $\mu_c$ , the Turing-Ising front hosts the Hopf mode in the front core (right inset). (b) Snapshot of a breathing Turing vortex. The Hopf mode  $B$  is damped everywhere in the plane, except at the Turing vortex core. Parameters:  $k_0 = 0.5$ ,  $\lambda = \kappa = 1$  and (a)  $\epsilon = 0.07$ ,  $\gamma_k = 0.03$ ,  $\nu = 0.01$ ,  $\alpha = 1 + 0.015i$ ,  $\beta = 1 + 0.06i$ ,  $\delta = 1 + 0.06i$ ,  $\gamma_\omega = 0$ , (b)  $\epsilon = 0.1$ ,  $\gamma_k = 0.0064$ ,  $k_0 = 0.5$ ,  $\mu = 0.089$ ,  $\nu = 0.05$ ,  $\alpha = 1$ ,  $\beta = 1 + 0.01i$ ,  $\delta = 1 + 0.01i$ ,  $\gamma_\omega = 0$ .

They lose stability to (longitudinal) Turing-Bloch fronts when  $\gamma_k$  is decreased below  $\epsilon/3$ . The Turing-Bloch fronts are given by

$$A = \sqrt{\Gamma} \tanh \left[ \sqrt{2\gamma_k} \left( \frac{x}{2k_0} \right) \right] \pm i \sqrt{\epsilon - 3\gamma_k} \operatorname{sech} \left[ \sqrt{2\gamma_k} \left( \frac{x}{2k_0} \right) \right], \quad B = 0, \quad (5)$$

and trace two types of trajectories connecting the two uniform states  $A = \pm\sqrt{\Gamma}$  in the complex  $A$  plane; clockwise (negative chirality) and anti-clockwise (positive chirality) [9].

In the mono-stability ranges considered here the uniform Hopf mode  $B$  is everywhere damped by the uniform Turing mode  $A$ . However, localized structures of the Turing mode, where  $|A|$  vanishes or is very small, may fail to damp the Hopf mode. The first example we consider is a longitudinal Turing-Ising front that vanishes at the front core ( $|A| = 0$  at  $x = 0$ ). Increasing  $\mu$ , the distance from the Hopf-bifurcation of the zero state, we identified a critical value,  $\mu_c$ , beyond which local temporal oscillations develop at the front core. This is a Hopf bifurcation of the stationary Turing-Ising front to a *breathing* Turing-Ising front. A numerically calculated bifurcation diagram of this instability is shown in fig. 2a. The insets in this figure show typical spatial profiles of the stationary and breathing Turing-Ising-fronts.

For the special case where  $\alpha = 4k_0^2$  and  $\beta = \delta = 1$ , we found an exact solution for the breathing Ising-front,

$$A = \sqrt{\Gamma} \tanh \left[ \sqrt{\Gamma - \mu} \left( \frac{x}{2k_0} \right) \right], \quad (6)$$

$$B = \sqrt{2\mu - \Gamma} \operatorname{sech} \left[ \sqrt{\Gamma - \mu} \left( \frac{x}{2k_0} \right) \right] e^{i\nu t + i\phi},$$

where  $\phi$  is an arbitrary constant phase. The solution appears at  $\mu_c = \Gamma/2$ . A transverse Turing-Ising front can go through a similar instability to a breathing front.

Another example of a localized Turing structure that can host the Hopf mode is a Turing vortex, where two Turing-Bloch fronts of opposite chirality meet. At the vortex core the Turing amplitude  $A$  vanishes and localized oscillations, giving rise to a *breathing Turing vortex*, can set in, as fig. 2 demonstrates for the case of longitudinal Turing-Bloch fronts. The critical  $\mu$  value where a breathing Turing vortex sets in is higher than that of a breathing Turing-Ising front.

The core lines of breathing Turing-Ising fronts in two space dimensions can be viewed as “self-organized waveguides” capable of propagating traveling waves. These core lines can host richer oscillatory dynamics when temporal forcing is added ( $\gamma_\omega \neq 0$ ). Forcing at a frequency twice as large as the breathing frequency locks the breathing phase at two stable values, shifted by  $\pi$  with respect to one another. A consequence of this bistability

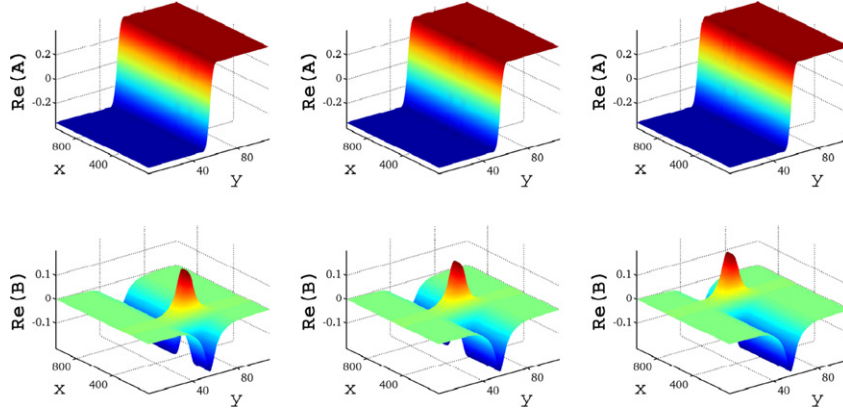


Fig. 3: Self-organized waveguide. Solution of eqs. (2) showing pulse propagation of the Hopf mode (bottom row) along the core line of a breathing Turing-Ising front in a system subjected to a spatial periodic forcing ( $k_f \approx 2k_0$ ) and a temporal periodic forcing ( $\omega_f \approx 2\omega_0$ ). Time proceeds from left to right. Note that the Turing mode (top row) is barely affected by the propagation of the Hopf pulse. Parameters:  $\epsilon = 0.05$ ,  $\lambda = \kappa = 1$ ,  $\gamma_k = 0.08$ ,  $k_0 = 0.5$ ,  $\mu = 0.103$ ,  $\nu = 0.001$ ,  $\alpha = 1$ ,  $\beta = 1$ ,  $\delta = 1$ ,  $\gamma_\omega = 0.003$ .

of phase states is the possible appearance of phase fronts along the core line of a breathing Turing-Ising front that shift the breathing phase by  $\pi$ . Depending on the strength of the temporal forcing,  $\gamma_\omega$ , the phase fronts can be stationary, resembling Ising fronts in homogeneous oscillatory media, or propagating, resembling Bloch fronts. Richer pattern formation phenomena, typical of homogeneous oscillatory media subjected to periodic forcing, may be expected as well. Figure 3 shows a pulse of the Hopf mode, consisting of a pair of (“Bloch”) phase fronts with opposite chirality, propagating along the core line of a transverse Turing-Ising front. Note that the front structure of the Turing amplitude  $A$  is hardly affected by the propagating pulse of the Hopf amplitude  $B$ .

Analogous behavior exist in mono-stability ranges of uniform pure Hopf solutions when the system is periodically forced in time rather than in space ( $\gamma_k = 0, \gamma_\omega \neq 0$ ). A stationary pure-mode Hopf-Ising front ( $A = 0, B = B_{Ising}(x)$ ) loses stability, as  $\epsilon$  is increased past a critical value to a mixed-mode Hopf-Ising front characterized by an amplitude  $A$  that does not vanish at the front core (the counterpart of the breathing Turing-Ising front)<sup>3</sup>. A propagating pure-mode Hopf-Bloch front ( $A = 0, B = B_{Bloch}(x - ct)$ ) can also lose stability to the growth of a localized Turing mode as fig. 4 demonstrates. The appearance of the Turing mode at the core of the Hopf-Bloch front beyond the instability point,  $\epsilon = \epsilon_{c1}$ , slows down the front motion as fig. 4b shows. Increasing  $\epsilon$  beyond a second threshold,  $\epsilon_{c2}$ , leads to a stationary front solution. As the insets in fig. 4a imply, the instability at  $\epsilon = \epsilon_{c2}$  takes a Bloch-type front at  $\epsilon < \epsilon_{c2}$ , where  $|B|$  does not vanish at the front core, to an Ising-type front at  $\epsilon > \epsilon_{c2}$ , where  $|B|$  does vanish at the front core. These results imply that a hidden Turing mode (*i.e.* linearly growing but nonlinearly

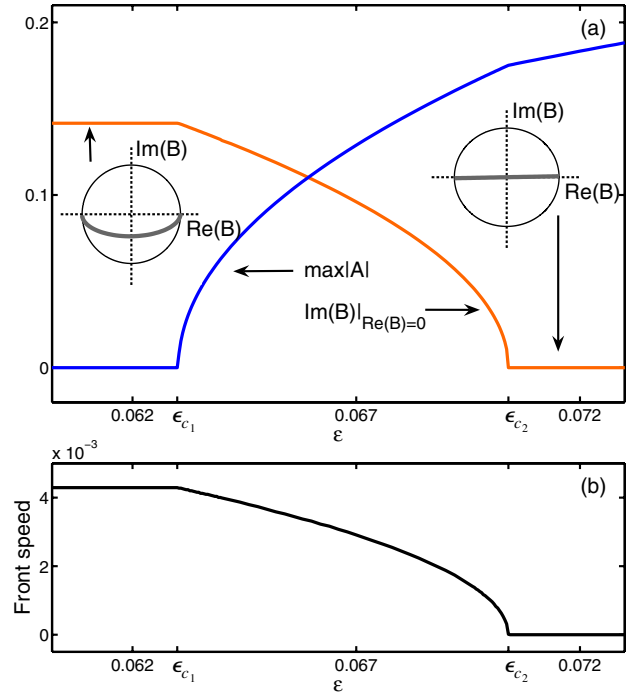


Fig. 4: Transition from a Hopf-Bloch front to a Hopf-Ising front induced by a hosted Turing mode. The transition is gradual and characterized by two thresholds:  $\epsilon_{c1}$ , designating the appearance of the Turing mode at the Bloch-front core and the slowing-down of the front motion, and  $\epsilon_{c2}$ , designating the transition to a non-propagating Ising front. Parameters:  $\lambda = \kappa = 1$ ,  $\gamma_k = 0$ ,  $k_0 = 0.5$ ,  $\mu = 0.1$ ,  $\nu = 0.001$ ,  $\alpha = 1$ ,  $\beta = 1.25$ ,  $\delta = 0.8$ ,  $\gamma_\omega = 0.025$ .

damped by a Hopf mode) can shift the threshold of a NIB bifurcation into the Bloch regime, making the Ising regime larger.

We focused our attention on localized structures (fronts, vortices) arising in periodically forced Hopf-Turing systems, but the general principles apply to other contexts as well. A topological defect, such as a

<sup>3</sup>For  $\alpha = 4k_0^2$ ,  $\beta = \delta = 1$  and  $\nu = 0$ , the critical value is  $\epsilon = (\mu + \gamma_\omega)/2$  and the solution is exactly the same as (6) when  $A$  and  $B$  are interchanged,  $\mu$  is replaced by  $\epsilon$  and  $\Gamma$  is replaced by  $\mu + \gamma_\omega$ .

dislocation defect in a spatially periodic pattern, can host an unstable oscillatory mode and give rise to a breathing defect similar in structure to that shown in fig. 2b. A nice experimental example is the observation of a spiral-core instability in Boussinesq Rayleigh-Bénard convection, beyond which a hexagonal mode appears at the core of a spiral-roll pattern [13]. In the context of biological communities, localized structures of a dominant species may host other species, forming spots of higher species diversity. Another potentially interesting ramification is data storage in localized structures [14]. Temporal forcing of a breathing vortex can provide a means for creating a multi-state vortex. Forcing at a frequency  $n$  times larger than the vortex breathing frequency yields  $n$  stable oscillation phases of the breathing vortex, thereby increasing the information content that can be stored in such a structure. Multi-state structures can also be formed by spatially forcing Hopf vortices and fronts that host the Turing mode. The existence of *traveling* Bloch fronts in this case (see the range  $\epsilon_{c_1} < \epsilon < \epsilon_{c_2}$  in fig. 4) can potentially be used for data transmission.

\*\*\*

The support of the James S. McDonnell Foundation is gratefully acknowledged.

#### REFERENCES

- [1] CROSS M. C. and HOHENBERG P. C., *Rev. Mod. Phys.*, **65** (1993) 851.
- [2] See, e.g., GROVER J. P., *Resource Competition* (Chapman and Hall, London) 1997.
- [3] REHBERG I. I. and AHLERS G., *Phys. Rev. Lett.*, **55** (1985) 500; ZIELINSKA B., MUKAMEL D. and STEINBERG V., *Phys. Rev. A*, **33** (1986) 1454; KOLODNER P., *Phys. Rev. E*, **48** (1993) R665.
- [4] CILIBERTO S. and GOLLUB J. P., *Phys. Rev. Lett.*, **52** (1984) 922; ARBELL H. and FINEBERG J., *Phys. Rev. Lett.*, **81** (1998) 4384.
- [5] DE KEPPER P., PERRAUD J. J., RUDOVICS B. and DULOS E., *Int. J. Bifurcat. Chaos*, **4** (1994) 1215; PERRAUD J. J., DE WIT A., DULOS E., DE KEPPER P., DEWEL G. and BORCKMANS P., *Phys. Rev. Lett.*, **71** (1993) 1272.
- [6] VORONTSOV M. A. and SAMSON B. A., *Phys. Rev. A*, **57** (1998) 3040.
- [7] DE WIT A., DEWEL G. and BORCKMANS P., *Phys. Rev. E*, **48** (1993) R4191; DE WIT A., LIMA D., DEWEL G. and BORCKMANS P., *Phys. Rev. E*, **54** (1996) 261; MEIXNER M., BOSE S. and SCHÖL E., *Physica D*, **109** (1997) 128; MEIXNER M., DE WIT A., BOSE S. and SCHÖL E., *Phys. Rev. E*, **55** (1997) 6690; TLIDI M., MANDEL P. and HAELTERMAN M., *Phys. Rev. E*, **56** (1997) 6524; TLIDI M. and HAELTERMAN M., *Phys. Lett. A*, **239** (1998) 59; NICOLA E. M., OR-GUIL M., WOLF W. and BÄR M., *Phys. Rev. E*, **65** (2002) 055101; YANG L., ZHABOTINSKY A. M. and EPSTEIN I. R., *Phys. Rev. Lett.*, **92** (2004) 198303; VANAG V. K. and EPSTEIN I. R., *Phys. Rev. Lett.*, **92** (2004) 128301-1; YOCHELIS A., ELPHICK C., HAGBERG A. and MERON E., *Europhys. Lett.*, **69** (2005) 170.
- [8] COULLET P., *Phys. Rev. Lett.*, **56** (1986) 724.
- [9] COULLET P., LEGA J., HOUCHEMANZADEH B. and LAJZEROWICZ J., *Phys. Rev. Lett.*, **65** (1990) 1352.
- [10] IKEDA H., MIMURA M. and NISHIURA Y., *Nonlin. Anal. Theory, Methods & Applic.*, **13** (1989) 507; HAGBERG A. and MERON E., *Nonlinearity*, **7** (1994) 805; BODE M., REUTER A., SCHEMELING R. and PURWINS H.-G., *Phys. Lett. A*, **185** (1994) 70.
- [11] HAGBERG A. and MERON E., *Phys. Rev. Lett.*, **78** (1997) 1166.
- [12] KORZINOV L., RABINOVICH M. I. and TSIMRING L. S., *Phys. Rev. A*, **46** (1992) 7601.
- [13] ASSENHEIMER M. and STEINBERG V., *Phys. Rev. Lett.*, **76** (1996) 756.
- [14] COULLET P., RIERA C. and TRESSER C., *Chaos*, **14** (2004) 193.